Reaction Chemistry & Engineering

Modelling for understanding the mechanism of hydrogen peroxide direct synthesis from batch, semibatch and continuous point of view

Journal:	*Reaction Chemistry & Engineering*
Manuscript ID	RE-ART-11-2015-000073.R1
Article Type:	Paper
Date Submitted by the Author:	26-Dec-2015
Complete List of Authors:	Gemo, Nicola; Abo Akademi, Salmi, Tapio; Abo Akademi University, Lab. of industrial Chemistry, Process Chemistry Centre Biasi, Pierdomenico; Åbo Akademi , Department of Chemical Engineering

Reaction Chemistry & Engineering

ARTICLE

Modelling for understanding the mechanism of hydrogen peroxide direct synthesis from batch, semibatch and continuous point of view

Nicola Gemo[a], Tapio Salmi[a], Pierdomenico Biasi[a,†]

Hydrogen peroxide direct synthesis was experimentally studied in three different reactors, namely batch, semibatch and trickle bed reactor (TBR), using a new promising catalyst based on Pd/K2621. Excellent results were obtained from the experimental point of view, achieving high H_2O_2 selectivities, around 90% at short contact time in batch, 60% in semibatch and 70% in TBR. The simplest rate equations compatible with the acknowledged reaction network have been included in a reactor model, which accounts for mass transfer resistances between gas and liquid of the liquid-catalyst surface. The corresponding Arrhenius parameters were estimated from direct synthesis experiments for all the reactions and reactors. The models show how the reaction rates change between batch, semibatch and trickle bed (TBR) reactors. Results suggest how to improve reactors set-up and reaction performances in continuous operations and how to compare the results between different reactors and conditions. The sensitivity analysis on the reaction allowed to gain new insights on the reaction rates. The TBR showed how the mass transfer limitations can help to direct the reaction towards the H_2O_2 synthesis. Remarkably, these results were achieved in the absence of any acids or halide ions, i.e. no known selectivity promoters for direct H_2O_2 synthesis were applied, thus the kinetics are not affected by the presence of promoters.

Introduction

The H_2O_2 direct synthesis (DS) is a simple but challenging reaction extensively studied in the last 20 years[1-4]. The simplicity of the DS comes from the fact that H_2 and O_2 dissolved in a reactant medium (e.g. methanol or water) react over a metallic supported catalyst to form H_2O_2, and the only byproduct is water. In principle, the DS aims at partially substitute the well established industrial autoxidation process (AO). The AO process counts some drawbacks such as the need for wastewater treatment, initial CAPEX, big industrial plants etc. The DS may solve these drawbacks but to be commercialized a high selectivity should be obtained. Indeed, the H_2O_2 produced in the DS is just an intermediate, and can be decomposed or hydrogenated to water by the same catalyst active for the DS[3] (Scheme 1).

The need to have an alternative to the AO process is strong enough to attract a lot of attention both from academia[4-7] and industry. The new century industry needs, in most of the cases, to reduce investment costs, to delocalize the production and to have flexible solutions with low waste management. Due to its potential, the DS is a process that will help to develop the new industry concept. Unfortunately, due to the lack of maturity in this research field, the real breakthrough is far and

the commercialization of the process still lags behind[4].
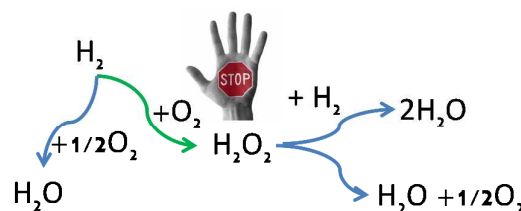
Scheme 1. Reactions involved in the direct synthesis of H_2O_2.

The above mentioned reasons are the driving forces that still make the DS a hot topic in the scientific community. Up to now the research in the direct synthesis is focused on the catalyst development[7-22], and only in the recent years the investigation on the entire process is gaining attention and importance[3, 23-29]. The publications that cover the catalyst development topic range from the study of the catalyst support, catalyst active metal, metal precursor and promoters in the reaction medium. Only recently, publications demonstrated the beneficial effect of studying the reaction from a chemical reaction engineering point of view[3, 5, 6, 30-32]. Indeed, it was demonstrated that playing with the reaction conditions and reactors set-up the performances of the catalyst can be enhanced. Despite the latest results, there are only some hypotheses on why the reaction conditions can ameliorate the DS. However, the attention should not be placed only on catalyst development

a. Department of Chemical Engineering, Åbo Akademi University, Biskopsgatan 8, ÅBO-TURKU, 20500, Finland.
† Corresponding author: bpierdom@abo.fi

or chemical reaction engineering, but the two approaches should be well integrated in a multidisciplinary research with a holistic approach[33]. Moreover, due to the extensive number of publications on the catalyst development, the comparison of results obtained is nowadays difficult due to the different systems (reactors and reaction conditions) used to test the catalysts. This problem is not trivial and up to now there is no solution on how to compare different data. In this regard a proper comparison is missing and the real state of the art can appear a little bit chaotic. These problems indicate the importance of a proper and fruitful connection between the chemistry and chemical engineering communities, filling the gap between them[33].

With this in mind, it was decided to study a novel promising catalyst[34] with three different reactors: batch, continuous stirring tank reactor (CSTR) and a trickle bed reactor (TBR)[3]. The choice of using a new catalyst comes from the fact that we have already demonstrated that playing with the reaction conditions, with a commercial catalyst, the DS reaction can be enhanced. The new catalyst was tailor made for the DS and it was developed, as the best practice for multiphase systems recommends, in a batch reactor, at fixed pressure, temperature and gas composition, to understand its performances[34]. After the first promising results, the catalyst was studied with different conditions in different reactors to clarify its performances, taking into consideration mass transfer, kinetics and to what extent the catalyst performances are affected by the different reactors. The choice to use batch, the CSTR (or semibatch) and TBR to study the kinetics comes from the fact that in our previous experience we qualitatively observed some phenomena such as the H_2/Pd ratio profile vs. H_2O_2 productivity, the H_2 mass transfer, the hydrogenation extent etc [3, 6, 9, 34, 35]. In this work the aim is to quantify these phenomena and to relate them to the different reactors used. With this approach the reaction was studied from the chemistry level to the chemical reaction engineering level, answering some of the still open issues in the DS. We also present here a powerful tool to understand how the different data in open literature can be compared between them. Understanding the reaction path and progress with the three reactors helps identify the strategies to improve the reaction conditions and the catalyst design. Moreover, understanding properly the reactors operation, the catalytic results can be evaluated with more criticism and the discovery of new insights will be faster.

Experimental

Materials

The catalyst was obtained by supporting palladium nanoparticles (0.5 wt.%) on a commercial PS-DVB macroreticular resin (Lewatit K2621), which proved to be an efficient support for the direct synthesis of hydrogen peroxide [17, 36, 37]. Details on the preparation via ion-exchange method are reported in our previous works [37, 38]. Pd(NO₃)₂ for the catalyst preparation was purchased from AlfaAesar. Sodium

thiosulfate pentahydrate (99.5%), potassium iodide, starch and concentrated sulfuric acid (all used for the peroxide titration) were purchased from Sigma-Aldrich; HPLC grade methanol (99.99%) from J.T. Baker; H_2, O_2 and CO_2 (99.999% mol/mol purity) from AGA (Linde group). Methanol for Karl Fischer titration, Hydranal composite 2 and ammonium molybdate tetrahydrate were purchased from Fluka. All materials were used as received. Complete characterization of the catalyst is reported in the supporting information.

Experimental setups

Using the same catalyst, experiments were carried out in three reactors: batch, semibatch and continuous (TBR). CO_2 was used to dilute the gas mixture outside flammability limits and to achieve a high H_2 solubility [39]. H_2O_2 and H_2O concentrations were determined at increasing time on stream by iodometric and Karl-Fischer titrations, respectively.

Batchwise experiments were performed in a 600 ml unbaffled reactor with standard geometry (Buchi), schematically represented in Figure 1.
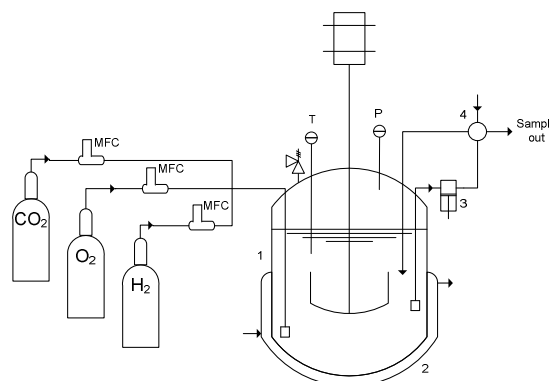
Figure 1. Schematic of the batch apparatus: 1, reactor; 2, cooling/heating jacket; 3, high pressure pump; 4, sampling valve; MFC, mass flow controller.

Experimental apparatus and procedures are described elsewhere [40]. Shortly, 0.15 g of the catalyst were loaded in the reactor. Carbon dioxide (20 bar) and oxygen (5 bar) were introduced in the vessel (298 K), followed by the injection of 400 ml of methanol. After pressure and temperature were stable at the desired values, hydrogen was fed as the limiting reagent. The reaction was assumed to start immediately after hydrogen loading. The gas mixture was carefully kept outside flammability. A stirring rate of 1000 rpm was conservatively adopted to ensure a good mixing of the liquid phase, as verified in dedicated experiments. The liquid phase was sampled from the batch reactor via a dedicated valve. Selectivity and conversion were calculated as:

$$S = 100 \frac{C_{H_2O_2}}{C_{H_2O_2} + C_{H_2O}} \qquad (1)$$

$$X_{H_2} = 100 \frac{C_{H_2O_2} + C_{H_2O}}{n_{H_2}^{IN}} V^L \qquad (2)$$

The semibatch experiments were performed in a 300 ml unbaffled reactor with standard geometry (Buchi) described elsewhere [41]. Figure 2 shows a schematic of the apparatus.
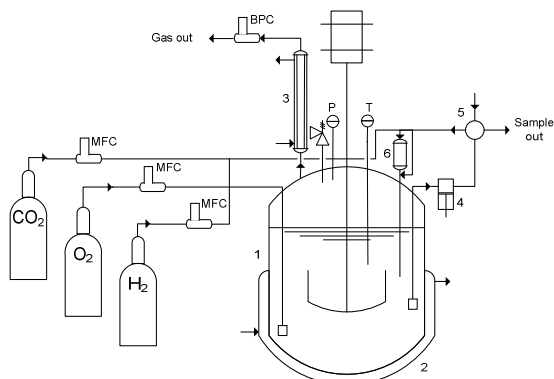
Figure 2. Schematic of the semibatch apparatus: 1, reactor; 2, cooling/heating jacket; 3, condenser; 4, high pressure pump; 5, sampling valve; 6, catalyst chamber; MFC, mass flow controller; BPC, back pressure controller.

Briefly, methanol (200 ml) was introduced in the vessel first, followed by the gas reagents. Throughout the experiments, the gas (300 Nml/min) was continuously bubbled into the static liquid with a 76-20-4 mol% composition in CO_2-O_2-H_2, respectively. The gas outlet was equipped with a condenser to ensure that no methanol left the reactor with the outgoing gas flow. The catalyst (0.2 g) was introduced last via a dedicated chamber, after the vapor-liquid equilibrium was reached at the desired temperature and pressure (20 bar). The reactions were assumed to start as the catalyst was lead into the reactor. Note that introducing the catalyst last allows for a very precise identification of the beginning of the reactions. The liquid phase was sampled via a dedicated valve and selectivity and conversion were calculated via equation (1) and (3), respectively:

$$X_{H_2} = 100 \frac{C_{H_2O_2} + C_{H_2O}}{\dot{n}_{H_2} \cdot t} V^L \qquad (3)$$

Continuous experiments were performed in a concurrent, downflow trickle bed reactor, developed from our previous apparatus [28]. A schematic of the reactor is shown in Figure 3.
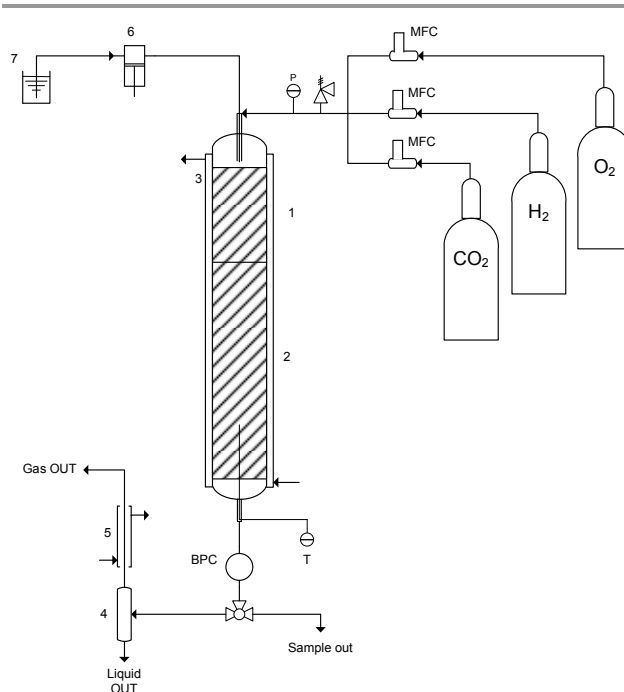
Figure 3. Schematic of the continuous TBR apparatus: 1, quartz sand; 2, catalytic bed; 3, cooling/heating jacket; 4, gas/liquid separator; 5, condenser; 6, high pressure pump; 7, methanol reservoir; MFC, mass flow controller; BPC, back pressure controller.

The reactor consisted of an AISI 316 stainless steel pipe, 50 cm long, with an internal diameter of 1.5 cm. A mixture of quartz sand/catalyst filling 30 cm of the reactor was introduced first, followed by pure quartz sand (15 cm) to ensure a good vapor-liquid equilibrium. Then methanol was flowed into the reactor (5 ml/min for 5 min) to wet the catalyst bed. Afterward the methanol flow was decreased at the desired rate and a mixture of CO_2 and O_2 was added. When stable pressure (20 bar) and temperature values were reached, H_2 was fed and the reaction assumed to start. The gas flow was 11 Nml/min with a composition of 73-23-4 mol% in CO_2-O_2-H_2, respectively. The liquid phase was sampled at increasing time on stream. Selectivity and conversion were calculated by equation (1) and (4), respectively:

$$X_{H_2} = 100 \frac{C_{H_2O_2} + C_{H_2O}}{\dot{n}_{H_2}^{IN}} \dot{V}^{L,IN} \qquad (4)$$

Models

Chemical kinetics

Several surface mechanisms on palladium can give the overall process described in Scheme 1. Voloshin et al. [32] screened some mechanisms to describe kinetic data obtained from microstructured reactors and concluded that a Langmuir-Hinshelwood-type mechanism, with the surface reaction steps as rate determining ones, gave the best agreement with experimental data. Dissociative adsorption of the reactant species was also proposed by Deguchi et al [42]. Some

mechanistic studies have given information about the reaction mechanism. For instance, Dissanyake and Lunsford [43] proposed that the O-O bond does not dissociate during the H_2O_2 synthesis process and Sivadinarayana et al. [44] confirm the species HO_2- on a gold catalyst surface. Wilson and Flaherty[45] proposed a detailed mechanism based on two site adsorption, where H2O2 forms by heterolytic reaction pathways resembling the two-electron oxygen reduction reaction (ORR). However, it is clear that water formation requires the rupture of the O-O bond on the catalyst surface. All these mechanism include several reaction constants, which are inevitably correlated when regression is attempted. Hence, in order to avoid overparameterization, no adsorption steps were included in the reaction mechanism; this assumption is also justified by the low reagent concentrations. Assuming that the reactions are irreversible, the simplest rate equations included in Scheme 1 are:

$$R_{ds} = k_{ds} C_{O_2}^L C_{H_2}^{L\,2} \tag{5}$$

$$R_{wf} = k_{wf} C_{O_2}^{L\,0.5} C_{H_2}^L \tag{6}$$

$$R_d = k_d C_{H_2O_2}^L \tag{7}$$

$$R_h = k_h C_{H_2O_2}^L C_{H_2}^L \tag{8}$$

with temperature dependent, Arrhenius-type kinetic constants:

$$k_i = A_i e^{-\frac{Ea_i}{RT}} \tag{9}$$

Pre-exponential factor (A_i) and activation energy (Ea_i) of each reaction are determined from our experimental data, as described below. According to Scheme 1, the production rates are obtained:

$$r_{H_2O_2} = R_{ds} - R_d - R_h \tag{10}$$

$$r_{H_2O} = R_{wf} + R_d + 2R_h \tag{11}$$

$$r_{H_2} = -R_{ds} - R_{wf} - R_h \tag{12}$$

$$r_{O_2} = -R_{ds} - 0.5R_{wf} + 0.5R_h \tag{13}$$

Mass balances

The mass balances developed for the mathematical models of the batch, semibatch and trickle bed reactors are described below.

Batch reactor

The reactor and operating procedures have been described elsewhere [31]. Shortly, it is a batch, slurry reactor with a self-inducing stirrer continuously drawing gas from the atmosphere above the liquid. The species mass balances have been written

in each phase, i.e. gas and liquid. Balances are based on the following assumptions:

 a) both liquid and gas phase are well mixed;
 b) carbon dioxide and methanol are not involved in any reaction;
 c) increment of liquid volume due to the accumulation of H_2O_2 and H_2O is neglected, while the change caused by sampling is taken into account.

Accordingly, the mass balances in the gas and liquid phases are:

$$\frac{dC_i^G}{dt} = -\frac{V^L}{V^G} k_i a^{LG} (C_i^{L,*} - C_i^L) \tag{14}$$

$$\frac{dC_i^L}{dt} = k_i a^{LG} (C_i^{L,*} - C_i^L) + \rho_B r_i \tag{15}$$

The liquid phase is assumed pseudo-homogeneous, so that the production rates r_i appear there and are assumed functions of the liquid phase concentrations (C_i^L). At the gas-liquid interface equilibrium holds:

$$C_i^{L,*} = C_i^G H_i \tag{16}$$

The equilibrium constants H_i depends on total composition, pressure and temperatures. Hi values are only needed for oxygen and hydrogen, due to assumptions (b) and (c), and are estimated from an equation of state tuned on specific experimental data [39]. The proposed model is given by a total of six ordinary differential equations, two for the gas phase and four for the liquid phase. Its integration yields the evolution in time of the concentration of reactants (H_2 and O_2) in the gas and liquid phases and of products (H_2O_2 and H_2O) in the liquid phase. According to the experimental procedure [40], the following six initial conditions are assumed:

$$(a)\ C_{O_2}^G\big|_{t=0} = C_{O_2}^{G,0}$$

$$(b)\ C_{H_2}^G\big|_{t=0} = \frac{n_{H_2}}{V^L}$$

$$(c)\ C_{O_2}^L\big|_{t=0} = C_{O_2}^{L,0} \tag{17}$$

$$(d)\ C_{H_2}^L\big|_{t=0} = C_{H_2O_2}^L\big|_{t=0} = 0$$

$$(e)\ C_{H_2O}^L\big|_{t=0} = C_{H_2O}^{L,0}$$

Hydrogen (the limiting reagent) was introduced after all the other species, when stable values of pressure and temperature were reached inside the reactor (filled with O_2, CO_2 and methanol). Since the H_2 feeding was fast compared to the reaction time [40], hydrogen is assumed not to dissolve in the liquid phase while introduced (conditions (17b) and (17c)). Initial compositions of the gas and liquid phases were evaluated with an equation of state [39]. The initial concentration of water in the reaction medium (condition (17e)) was measured prior the introduction of hydrogen [40]. The material balances, eqs.(14) and (15), together with initial conditions (17), have been efficiently solved using Matlab's "ode15s" solver, also suitable for stiff equations, being based

on a multistep, variable order method based on the numerical differentiation formulas.

Semibatch reactor

The semibatch is a slurry reactor, similar to the batch previously described. Here gas reagents were continuously fed via three mass flow controllers. The pressure was kept constant via a back pressure controller. Mass balances are based on the following assumptions:

a) both liquid and gas phase are well mixed;
b) carbon dioxide and methanol are not involved in any reaction;
c) any increment of liquid volume due to the accumulation of H_2O_2 and H_2O is neglected, while the change caused by sampling is taken into account;
d) the gas composition at the outlet is assumed equal to the composition inside the reactor (i.e. the gas phase behaves like a continuous stream tank reactor);
e) the gas mixture is assumed ideal, i.e. the density does not depend on composition.

Accordingly, the mass balances in the gas and liquid phases can be written as:

$$\frac{dC_i^G}{dt} = \frac{\dot{n}_{Tot}^{IN} C_i^{IN}}{V^G \rho^G} - \frac{C_i^G \dot{n}_{Tot}^{OUT}}{V^G \rho^G} - \frac{V^L}{V^G} k_i a^{LG} \left(C_i^{L,*} - C_i^L\right) \quad (18)$$

$$\dot{n}_{Tot}^{OUT} = \dot{n}_{Tot}^{IN} - \sum_i^{nc} V^L k_i a^{LG} \left(C_i^{L,*} - C_i^L\right) \quad (19)$$

$$\frac{dC_i^L}{dt} = k_i a^{LG} \left(C_i^{L,*} - C_i^L\right) + \rho_B r_i \quad (20)$$

where the liquid phase is again assumed pseudo-homogeneous and at the gas-liquid interface equilibrium holds, eq. (16). Once again, H_i values [39] are only needed for oxygen and hydrogen (assumptions (b) and (c)) and production rates r_i are functions of the liquid phase composition (C_i^L). Note that the gas density is constant, because of assumption (e) and constant T and P. The proposed model is given by a total of seven equations: two ordinary differential equations and one algebraic equation for the gas phase and four ordinary differential equations for the liquid. Its integration yields the evolution in time of the concentration of reactants (H_2 and O_2) in the gas and liquid phases, of products (H_2O_2 and H_2O) in the liquid phase and the total molar flow at the reactor outlet. According to the experimental procedure, the following seven initial conditions are assumed:

$$(a) \left. C_i^G \right|_{t=0} = C_i^{G,0} \qquad i = O_2, H_2$$

$$(b) \left. C_i^L \right|_{t=0} = C_i^{L,0} \qquad i = O_2, H_2, H_2O_2, H_2O \quad (21)$$

$$(c) \left. \dot{n}_{Tot}^{OUT} \right|_{t=0} = \dot{n}_{Tot}^{IN}$$

The catalyst was introduced last, when stable values of pressure and temperature were reached inside the reactor (filled with H_2, O_2, CO_2 and methanol). Initial compositions of the gas and liquid phases were evaluated with an equation of state [39]. The initial concentration of water in the reaction medium (condition (21b)) was measured prior the introduction of the catalyst. The material balances eqs. (18)-(20), together with initial conditions (21), give a mixed algebraic-differential equations (ADE) system, which have been efficiently solved using Matlab's "ode15s" ADE solver.

Trickle bed reactor

In the trickle bed reactor, both gas and liquid were continuously fed via three mass flow controllers and a high pressure pump, respectively. The model is based on an advances approach reported in our previous study on the fluid dynamic of a trickle bed reactor [46]. The liquid flow is described by a combination in series of axial dispersion (ADM) and a stirred tank (ST) model, whereas the gas phase is described by a plug flow model. A schematic representation is given in Figure 4.
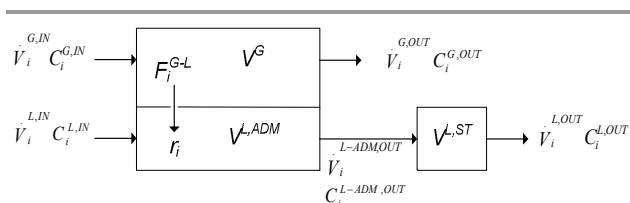
Figure 4. Schematic representation of the trickle bed reactor model.

Balances are based on the following assumptions:

a) carbon dioxide and methanol are not involved in any reaction;
b) any increment of liquid volume due to the accumulation of H_2O_2 and H_2O is neglected;
c) steady state conditions;
d) the reactions only occur in the ADM liquid volume;
e) the ST liquid volume is isolated from the gas phase;
f) constant pressure.

Accordingly, the mass balances in the gas and liquid phases are:

$$\frac{d^2 C_i^{L,ADM}}{dz^2} = \frac{L v_L}{\mathcal{D}} \frac{dC_i^{L,ADM}}{dz} - \frac{L^2}{\mathcal{D}} k_i a^{LG} \left(C_i^{L,*} - C_i^{L,ADM}\right) - \frac{L^2}{\mathcal{D}} \rho_B^{ADM} r_i \quad (22)$$

$$\frac{dC_i^G}{dz} = -\frac{V^{L,ADM} L}{V^G v_G} k_i a^{LG} \left(C_i^{L,*} - C_i^{L,ADM}\right) \quad (23)$$

$$\frac{dC_i^L}{dz} = C_i^{L,ADM} - C_i^L \quad (24)$$

where

$$(a) \; v_L = \frac{L\dot{V}^L}{V^{L,ADM}}$$

$$\text{(25)}$$

$$(b) \; v_G = \frac{L\dot{V}^G}{V^G}$$

The liquid phase in the ADM model is again assumed pseudo-homogeneous and equilibrium holds at the gas-liquid interface (eq. (16), only necessary for oxygen and hydrogen). According to assumption (d), the production rates r_i are a function of the concentrations in the ADM model ($C_i^{L,ADM}$), and hence the catalyst density (ρ_B^{ADM}) is referred to the ADM liquid volume. Note that the accumulation term in the ST model, eq. (24), was referred to the spatial coordinate in the ADM model:

$$\frac{dC_i^L}{dt^{ST}} = \frac{dC_i^L}{d\left(\tau^{ST}\frac{l}{L}\right)} = \frac{dC_i^L}{\tau^{ST}dz} = \frac{\dot{V}^L}{V^{L,ST}}\frac{dC_i^L}{dz} \qquad (26)$$

In eq. (22) the axial dispersion coefficient ($\mathcal{D}$) appears. Its value was calculated according to the following correlation [46], based on specific residence time distribution measurements:

$$Pe = \left(916061.7 + 6063.5Re_{Gp}\right)\frac{Re_{Lp}^{0.571}}{Ga} \qquad (27)$$

The volume of the liquid ($V^{L,ADM}$ and $V^{L,ST}$) and gas phases (V^G) were calculated as follow:

$$V^{L,ADM} = \frac{L\theta^{ADM}\dot{V}^L}{u_L + u_g} \qquad (28)$$

$$V^{L,ST} = \frac{L\theta^{ST}\dot{V}^L}{u_L + u_g} \qquad (29)$$

$$V^G = \varepsilon\pi R^2 L - \left(V^{L,ADM} + V^{L,ST}\right) \qquad (30)$$

where the dimensionless residence time in the ADM and ST models (ϑ^{ADM} and ϑ^{ST}, respectively) were calculated according to the following correlations [46]:

$$(a) \; \theta^{ADM} = 0.547\left(1 + \frac{u_G}{u_L}\right)$$

$$\text{(31)}$$

$$(b) \; \theta^{ST} = 0.095\left(1 + \frac{u_G}{u_L}\right)$$

The model calculates the compositions along the reactor length at the steady state condition (assumption (c)), so that the time dependence is not taken into account. Therefore, eqs. (22)-(24) represent a boundary value problem, which requires the following boundary conditions:

$$(a) \; u_L C_i^L\big|_{z=0^-} = u_L C_i^L\big|_{z=0^+} - \frac{\mathcal{D}}{L}\frac{dC_i^L}{dz}\bigg|_{z=0^+} \qquad (32)$$

$$(b) \; \frac{dC_i^L}{dz}\bigg|_{z=1} = 0$$

$$(c) \; C_i^G\big|_{z=0} = C_i^{G,IN}$$

$$(d) \; C_i^{L,ADM}\big|_{z=0} = C_i^L\big|_{z=0} = C_i^{L,IN}$$

Danckwerts conditions were chosen for eq. (22), i.e. continuous flow at the reactor inlet (condition (32a)) and zero slope condition at the reactor exit (condition (32b)). Gas phase composition at the reactor inlet (condition (32c)) was imposed via the three mass flow controllers. Reagents liquid composition at the reactor inlet (condition (32d)) was evaluated with an equation of state[39], whereas water was measured in the methanol reservoir.

The proposed model is given by a total of ten equations: four ordinary differential equations and four second order ordinary differential equations for the liquid phase and two ordinary differential equations for the gas. Its integration yields the evolution along the reactor length of the concentration of reactants (H_2 and O_2) in the gas and liquid phases and of products (H_2O_2 and H_2O) in the liquid phase. The material balances eqs. (22)-(24), together with boundary conditions (32), have been efficiently solved using Matlab's "bvp5c" solver for boundary value problems, a finite difference code that implements the four-stage Lobatto IIIa formula as an implicit Runge-Kutta method.

Kinetic identification

The kinetic models have been formulated above. The values of the activation energy (Ea) and pre-exponential factor (A) of each reaction involved were determined by isothermal experimental data fitting. The four irreversible reaction rate constants k_{ds}, k_{wf}, k_d and k_h were individually regressed at the given temperatures, minimizing the following error function:

$$err_T = \frac{\sqrt{\sum_{j=1}^{N_{H_2O_2}^{exp}}\left(C_{H_2O_2,j}^{L,exp} - C_{H_2O_2,j}^{L,calc}\right)^2}}{1/N_{H_2O_2}^{exp}\sum_{j=1}^{N_{H_2O_2}^{exp}}C_{H_2O_2,j}^{L,exp}}\Bigg|_T$$
$$+ \frac{\sqrt{\sum_{j=1}^{N_{H_2O}^{exp}}\left(C_{H_2O,j}^{L,exp} - C_{H_2O,j}^{L,calc}\right)^2}}{1/N_{H_2O}^{exp}\sum_{j=1}^{N_{H_2O_2}^{exp}}C_{H_2O,j}^{L,exp}}\Bigg|_T \qquad (33)$$

Note that errors between experimental and calculated concentrations have been rescaled. The Ea and A values were then assessed by fitting $k(T)$ with the Arrhenius equation. A Nelder-Mead simplex algorithm with positive constrains on the parameters (a modification of the Matlab function "fminsearch") was used to minimize the error by adjusting the parameters of the model.

The results were critically analyzed by preparing sensitivity plots, in which the objective function was plotted as a function of a single parameters at a time, while the other parameter

values were kept fixed, which gave the objective function minimum. The correlation between the parameters are visualized evaluating a contour plots for each pair, that is plotting couples of parameter values that result in the same value of the error function (33), with the other parameters kept constant (Supporting Information, Figures S.3-S.7).

Experimental results

Experiments were carried out in batch, semibatch and trickle bed reactors at temperatures in the range -10 to 30 °C. Results are reported below for each of the experimental set up investigated.

Batch reactor

Experimental results obtained in the batch reactor are reported in Figure 5 as H_2O_2 and H_2O concentrations, selectivity and H_2 conversion at different temperature values. All experiments were carried out within the kinetic regime, as demonstrated in our previous works [31, 40].
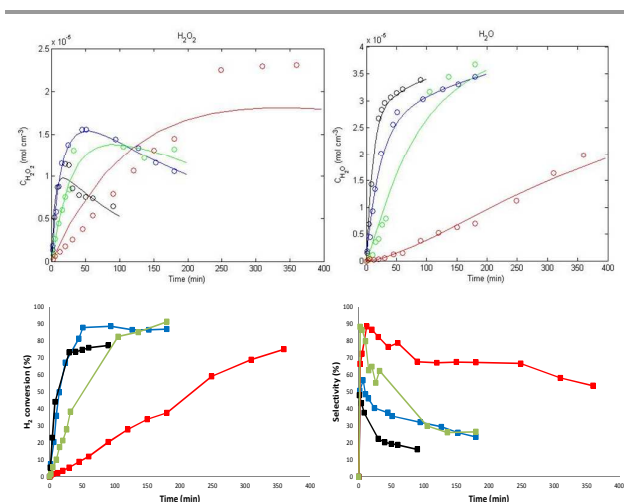
Figure 5. H_2O_2 and H_2O concentrations (top left and right, respectively), selectivity (bottom right) and H_2 conversion (bottom left) as a function of time on stream in the batch reactor: ■, -10 °C; ■, 2 °C; ■, 15 °C; ■, 30 °C. Solid lines represent the model.

Water concentration increased constantly, prevailing over the hydrogen peroxide concentration only at the higher temperatures (15 and 30 °C). H_2O_2 concentration rapidly increased for short contact time, reaching a maximum and gradually decreasing afterwards. A complete consumption of H_2 (the limiting reagent) corresponded to the maximum concentration of H_2O_2: after H_2 was no longer present in the liquid phase, the direct synthesis as well as the hydrogenation were suppressed and thus only the decomposition of H_2O_2 took place; this resulted in a drop of the peroxide formation and consequently in a slower water production rate. Interestingly, H_2O_2 concentration decreased with temperature, whereas the opposite effect was observed on H_2O. This resulted in a higher selectivity at lower temperatures, with values up to 90% at -10 and 2 °C and short contact time. Note

also that the selectivity decreased with increasing temperature at the same H_2 conversion. Moreover, the H_2O concentration rapidly increased also for very short contact time. These observations suggest that a) the direct formation of water is immediately competitive with the H_2O_2 direct synthesis reaction and b) the activation energy of the direct synthesis and the dominant H_2O production reactions are very different, the former likely being lower than the latter.

Semibatch reactor

Experimental results obtained in the semibatch reactor are reported in Figure 6 in terms of H_2O_2 and H_2O concentrations, selectivity and H_2 conversion at different temperatures. Mass transfer limitations in the reactor were investigated in our previous work [41], concluding that experiments were performed within the kinetic regime.
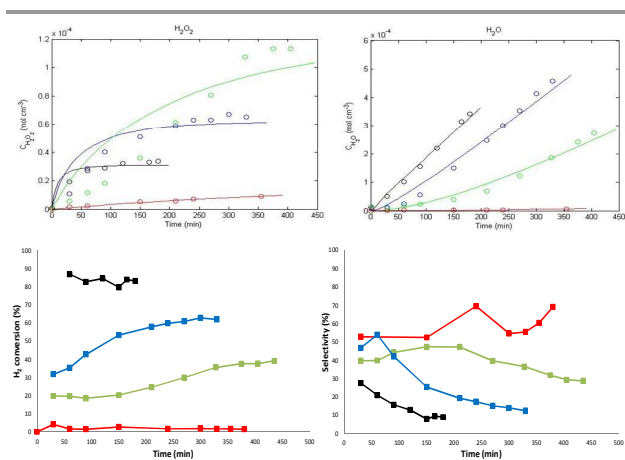
Figure 6. H_2O_2 and H_2O concentrations (top left and right, respectively), selectivity (bottom right) and H_2 conversion (bottom left) as a function of time on stream in the semibatch reactor: ■, -10 °C; ■, 2 °C; ■, 15 °C; ■, 30 °C. Solid lines represent the model.

In all experiments, the H_2O_2 concentration leaned towards a steady state value, and at the same time the H_2O concentration steadily increased. This was expected, since H_2O_2 is a reaction intermediate and water is the final product; in a semibatch apparatus the accumulation of peroxide leads to an increase of hydrogenation and disproportionation rates, so that H_2O_2 concentration reaches a steady value, whereas water concentration increases. Selectivity values decreased with temperature and time on stream, as for the batch apparatus (Figure 5), though higher values were achieved in that reactor. As for the batch reactor, H_2O_2 decreased with temperature, whereas H_2O increased. Hence, selectivity toward the peroxide decreased with H_2 conversion, as expected for an intermediate product (Scheme 1). Interestingly, H_2 conversion increased with the time on stream; moreover, H_2O production was slow at the beginning and increased with time on stream. These observations suggest that: a) the H_2O_2 direct synthesis is more favored than the H_2O production reaction (in contrast to the batch reactor, where H_2O production was fast also at short time on stream); b) as for the batch reactor, the activation energy of the direct

synthesis and the dominant H_2O production reactions are very different, the former being likely lower than the latter; c) hydrogenation is the preferred reaction for H_2O production, because of observation a) and the increasing H_2 conversion with the time on stream.

Trickle bed reactor

Experiments in the TBR were carried out with constant catalyst amount (0.2 g) with two liquid flow rates (LFR) and increasing temperature. Results are reported in Figure 7 in terms of H_2O_2 and H_2O concentrations at steady state.
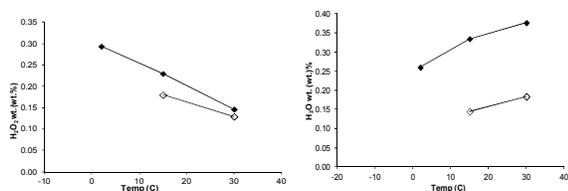
Figure 7. H_2O_2 (left) and H_2O (right) concentrations at steady state as a function of temperature at different LFR: ♦, 1.75 ml/min; ◊, 3 ml/min. Catalyst amount 0.2 g.

As observed in the batch and semibatch experiments, the H_2O_2 concentration decreased with temperature, whereas H_2O increased. This confirmed the hypothesis that the activation energy of the direct synthesis reactions is likely lower than the one of the dominant H_2O production reaction. As a consequence, the selectivity decreased with the H_2 conversion, as shown in Figure 8. These results were qualitatively independent of the liquid flow rate. However, increasing methanol flow rate resulted in a lower H_2O_2 and H_2O production (Figure 7), due to the reduced contact time. The data are actually consistent in terms of selectivity and H_2 conversion, as shown in Figure 8.
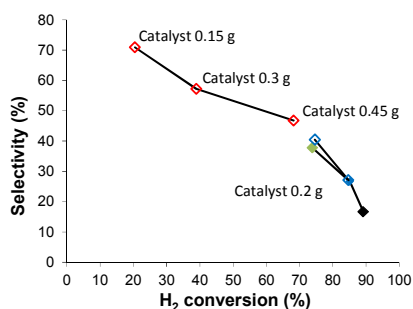
Figure 8. Selectivity as a function of H_2 conversion at steady state in the trickle bed reactor at LFR 1.75 ml/min (full symbols) and 3 ml/min (void symbols): ♦, -10 °C; ♦, 2 °C; ♦, 15 °C; ♦, 30 °C.

The H_2 conversion values obtained in the TBR were between 20 and 98%, a range more limited than those obtained in the other series of experiments (Figure 5 and Figure 6). In order to get a better comparison with the data obtained in the batch and semibatch apparati, data at lower H_2 conversion are desirable. Hence, experiments were carried out at the lowest temperature (-10 °C) with increasing catalyst amount (LFR = 3 ml/min). Results are reported in Figure 9.
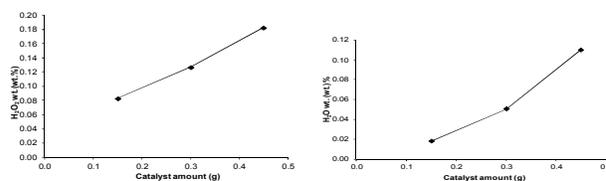
Figure 9. H_2O_2 (left) and H_2O (right) concentrations at steady state as a function of catalyst amount. FLR 3 ml/min and -10 °C.

As expected, H_2O_2 and H_2O concentration linearly increased with the catalyst amount in the reactor. Selectivity and H_2 conversion (Figure 8) are consistent with the data measured at different temperature, and liquid flow rates, with selectivity values up to 71% at 20% H_2 conversion.

Discussion

In order to quantitatively compare the experimental results, the kinetic parameters of the catalyst have been regressed using the experimental data in the three reactor set-ups investigated. The calculated activation energies and pre-exponential factors of all reactions involved (Scheme 1) are reported in Table 1.

Table 1. Activation energy and pre-exponential factors regressed in the batch, semibatch and continuous experiments. ds = direct synthesis, wf = direct water formation, d = decomposition and h = hydrogenation.

	Batch		Semibatch		TBR	
	Ea	A	Ea	A	Ea	A
	kJ/mol		kJ/mol		kJ/mol	
ds	42.6	1.47E+09	67.0	8.90E+21	6.9	3.18e+17
wf	92.3	4.38E+23	133.8	1.15E+14	8.0	5.52e+15
d	30.1	1.47E+09	58.9	1.09E+20	5.1	4.66e+3
h	53.2	1.38E+19	29.8	7.07E+02	7.3	3.87e+15

The rate of each reaction was also calculated. Results are shown in Figure 10 as ratios between the rate of the undesired reactions (water formation, hydrogenation and disproportionation) and the direct synthesis reaction rate, so to mark the favoured undesired reaction.
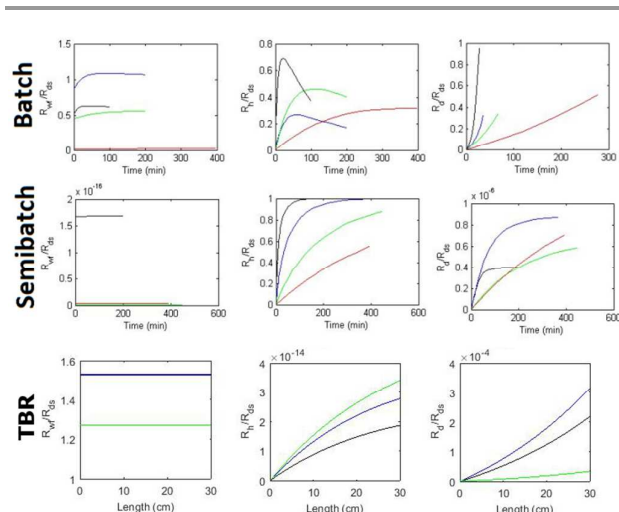
Figure 10. Ratios between water formation, hydrogenation, disproportionation and direct synthesis reaction rates in batch, semibatch and TBR experiments. ■, -10 °C; ■, 2 °C; ■, 15 °C; ■, 30 °C. R_{ds}, rate of direct synthesis, R_{wf}, rate of water formation, R_h, rate of hydrogenation of hydrogen peroxide, R_d, rate of decomposition of hydrogen peroxide.

In the batch reactor, all the kinetic parameters were well identified, as the sensitivity analysis reveals (Supporting information, Figure S.3). The contour plots (Supporting information, Figure S.4) show some correlation between the parameters, especially among water formation and hydrogenation, but this is expected, given the complex scheme of reaction. As qualitatively noticed in the previous section, in the batch reactor water formation competes with the direct synthesis reaction (Figure 10); however, the ratio R_{wf}/R_{ds} is larger than 1 only for the highest temperature, i.e. the water formation reaction prevails over the direct synthesis only at high temperature; at the same time, also the hydrogenation and decomposition reactions are significant, although both the R_h/R_{ds} and R_d/R_{ds} ratios had values lower than 1. The direct synthesis activation energy is confirmed to be lower than that of water formation (Table 1).

Data collected in the semibatch apparatus were somewhat different. The sensitivity analysis (Supporting information, Figure S.5) reveals that water formation and decomposition reactions had a negligible effect on the objective function; this confirms that the reaction rate of water formation and disproportionation reactions were negligible compared to the direct synthesis rate, as actually shown in Figure 10. The contour plot (Supporting information, Figure S.6) reveals a slight correlation between the direct synthesis and hydrogenation reaction. As noticed in the previous section, the most important reaction competing with the direct synthesis was the hydrogenation, although R_h/R_{ds} values were always lower than 1 (Figure 10). The activation energy of water formation was higher than that of the direct synthesis reaction, as noticed in the batch reactor (Table 1). However, two major differences are apparent when comparing results in the batch and semibatch reactor: 1) in the batch apparatus all the undesired reactions were competing with direct synthesis, whereas in the semibatch only hydrogenation had a significant

effect (Figure 10); 2) although the activation energy of direct synthesis was lower than that of water formation, values obtained in the two apparatus were quite apart (Table 1). These observations suggest that the reaction conditions affect the catalyst performance. In the batch reactor, the reagents were only fed at the beginning, so they slowly decreased during the course of the reaction; in particular, the concentration of H_2 (the limiting reagent) widely decreased with the time on stream. In the semibatch reactor the reagents concentrations were constant instead. This difference is likely to affect the catalyst morphology; it is known that the oxidation state of a catalyst has an effect on the reaction rates[16, 34, 38, 47-50]. In the semibatch reactor, the H_2 concentration in the liquid phase was constant and higher than in the batch apparatus (where it decreased with the time on stream), possibly causing the observed differences in the reaction rates (Figure 10) and activation energies (Table 1).

In the trickle bed reactor, the kinetic parameters were apparently well identified, as the sensitivity analysis reveals (Supporting information, Figure S.7); the hydrogenation reaction had little effect on the objective function (Supporting information, Figure S.7), meaning that its rate was much slower compared to the other reactions. This is confirmed by the reaction rate ratios reported in Figure 10, where the hydrogenation reaction rate is much lower than that of the direct synthesis reaction (R_h/R_{ds} values much lower than 1). Figure 10 also reveals that the disproportionation reaction was much slower than the direct synthesis (R_d/R_{ds} values much lower than 1). As qualitatively noticed in the previous section, the activation energy of the direct synthesis (Table 1) is lower than the water formation activation energy (the main responsible of water production, as Figure 10 shows). However, the activation energy values of all the reaction was very low (< 10 kJ/mol). This means that the temperature had little effect on the reaction rates, suggesting that the experiments were carried out with some mass transfer limitations. Notwithstanding, other considerations on the different activation energies obtained can be derived from the reactors and their features. Indeed, In the TBR the liquid residence time and the gas residence time can be controlled separately while in Batch and Semibatch this is not possible. For example, in the TBR the liquid residence time is very low, keeping the conversion low and thus avoiding the consecutive reactions (the catalyst is in contact with the liquid phase for a limited amount of time). In the Batch and Semibatch reactors the liquid residence time is fixed, only H_2, the limiting reagent, can be fed with different velocities. Thus if the H_2 feeding is fast the H2 conversion is low, otherwise the opposite. In the Semibatch reactor the liquid phase is saturated by H_2, and H_2 is always present (the value of H_2 in the liquid phase depends on the H2 conversion). Despite a low H_2 conversion the H_2O_2 produced is surrounded by high concentration of H2, and this can result in a high hydrogenation rate. In any case the liquid phase has always a fresh H_2 refilling, so hydrogenation (and decomposition) are highly probable (to different extent) due to the simultaneous presence of H_2 and H_2O_2. On the opposite TBR and Batch reactor behave differently due to the different

reaction conditions (as explained above). Thus mass transfer can be one explanation, but also the residence time and H_2 presence in the liquid phase play an important role in the reaction pathway. In this way the different parameters obtained can be ascribed to the different reaction conditions that can affect the nanoclusters features, as already reported[34]. Hence, care must be taken when carrying out experiments in this kind of continuous apparatus. Higher space velocities are needed to operate free from mass transfer limitations in continuous reactors. It is important to underline that we saw for the first time that the hydrogenation and decomposition reactions can be avoided if the reactor operates in mass transfer, however in the conditions studied the direct water formation prevail. In semibatch, where the concentration of H_2 in the liquid phase is stable the direct formation is almost avoided. A continuous reactor with multiple H_2 injection would favor the H_2O_2 production, as we saw here (and previously) that the saturation of H_2 in the liquid phase is beneficial for the reaction. Of course, a deep analysis on where to add the feed injections, how much hydrogen should be added and the catalyst amount to be used, should be a matter of a future study. Despite this, the work on the catalyst design should also focus on how to tailor made the porosity of the catalyst to balance the mass transfer inside the pores in order to enhance the direct synthesis.

Remarkably, these results were achieved in the absence of any acids or halide ions, i.e. no known selectivity promoters for direct H_2O_2 synthesis were applied. The kinetics express the real potential of the catalyst, thus the guidelines for the catalyst design can be given avoiding misinterpretations on the catalyst activity.

Proposed Mechanism

The possible mechanism that can be speculated from the present results and from previous discoveries[31,34] take into considerations the following behavior of Pd.

It is interesting to note that the PdO seems detrimental for the H_2O_2 direct synthesis and that there is a competitive adsorption between H_2 and O_2 on the Pd surface[34]. H_2 adsorption on the Pd surface is favoured compared to O_2 [34]. Moreover, the presence of PdO can be found also after the reaction on the catalyst surface[34]. The degree of the oxidation kinetics of Pd surfaces was found to be correlated with temperature and with the crystal type of Pd[51,52,53,54,55,56,57,58]. Pd(111) nucleation is thermodynamically controlled, and therefore, the nucleation rate decreases with temperature. On Pd(110), nucleation is predominantly kinetically controlled and thus the oxidation rate increases with temperature[52]. PdO species can be thus nucleated[52], and what it was seen in a previous study was that a higher degree of oxidation favours water formation[34]. O_2 can be molecular bonded to PdO[51,52], and this molecule can be active in CO oxidation[51]. PdO_2 species exists on the surface of PdO[52]. On Pd (100) the O_2 adsorption can lead to a phase transformation and reconstruction[53]. The activation energies for CO oxidation (for the Langmuir–Hinshelwood steps) was found different with large oxygen

coverage and large CO coverage[56]. Taking into consideration the behavior of O_2 coverage on palladium it can be derived from the previous cited studies that the activation energies can depend on the oxidation degree of the Pd surface as noted in[56]. Thus, our different activation energies obtained in the TBR can be ascribed to a different oxidation state of the Pd clusters compared to the Batch or Semibatch case. This is highly probable since the catalyst surface in the TBR has a shorter contact time with H_2O_2, the opposite of what happens in Batch and Semibatch conditions. Despite this, from the present results, it can not be ruled out which is the form of the Pd oxidation state in the TBR. What can be said about the mechanism is that probably water formation is correlated to the oxidation degree of Pd and that the process passes through an intermediate on the PdO surface. Most likely O_2 can be activated on PdO surface, rather than hydrogen that has its activation step on Pd^0 surface. H_2 reacts with the PdO_2 complex that can be formed[52], leading to water formation. O_2 can be molecular or atomic adsorbed on PdO and Pd^0, thus the Pd^0 surface, in principle, can promote both direct synthesis and direct water formation. It has to be kept into consideration that depending on the Pd crystallography faces the reaction of direct synthesis can be enhanced or reduced. From our previous study[34] it seems that water formation can be suppressed using catalysts with a low amount of Pd (they result in low PdO oxidation state). Most probably H_2O_2 direct synthesis mechanism depends on the surface coverage, that is regulated by temperature, Pd amount and H_2/O_2 ratio in the liquid phase. What is important to take into account is the fact that hydrogen solubility is the opposite compared to the other gases: the lower the temperature, the higher the H_2 solubility. This fact helps keeping the surface oxidation state as Pd^0 at low temperatures. The feature of H_2 solubility helps in speculating that the coverage of the Pd at low temperature has a large H_2 coverage while at high temperatures the oxygen coverage on the Pd surface is more favored (e.g. at low temperatures: higher H_2 solubility and lower O_2 solubility coupled with a favored adsorption of H_2 compared to O_2 on Pd surface). Indeed, our results confirm that H_2O_2 is more favored at low temperatures compared to relative high temperatures. The Activation Energies calculated from our experiments may reflect the different H_2/O_2 ratio in the liquid phase (in the different reactors) and thus different Pd oxidation state. This analysis coupled with our present and past results lead to the suggestion that the direct water formation can be ascribed to the H_2 combustion on PdO surface. On the opposite, the H_2O_2 hydrogenation reaction is more difficult to understand. It seems that hydrogenation is predominant when H_2 combustion rate is low, thus it may happen on Pd^0 surface. The reaction involves the H_2 adsorption and H_2O_2 adsorption on Pd surfaces. Most probably here the probability of H_2O_2 adsorption is due to two main factors: 1) competitive adsorption of H_2O_2 with O_2/H_2, 2) H_2O_2 concentration. In the Semibatch reactor hydrogenation is important, since the concentration of H_2O_2 increases with time. Moreover, as can be seen from the activation energies, the reaction is highly favored. The mechanism for the H_2O_2 direct synthesis can be

similar to the one proposed by Wilson and Flaherty[45] with two site adsorption, but with more focus on the Pd oxidation state as responsible for the water formation with a complimentary role of the nanocluster size, as similarly reported also by Ouyang et al.[59]. The mechanism discussed is in line with our findings (activation energies and pre-exponential factors) in batch, semibatch and TBR. Despite this it will be important to monitor more deeply the Pd oxidation state evolution during the reaction, at different operative conditions, to make a further step in the direct synthesis. There is another issue that was never discussed in the H_2O_2 direct synthesis: the O_2 sorption on the Pd subsurface[56]. The bulk and subsurface oxygen can influence the catalytic activity being directly or indirectly involved in the reaction as studied in the CO oxidation[56]. It is still difficult to claim the role of the O_2 sorption in the direct synthesis, but is something that in the future should be considered. The present work may help in individuating particular reaction conditions that can be studied to implement a more detailed model that take into consideration: 1) PdO oxidation state and its role on the water formation, 2) competitive adsorption of H_2/O_2 3) subsurface and bulk O_2 in the palladium clusters 4) β-hidrides that can influence the reaction 5) the use of a model that involves different sites adsorption for the reactions involved and 6) a dynamic approach of the nanocluster evolution during the direct synthesis. Although there are still some unclear phenomena that regulate the direct synthesis, new insights are appearing for a complete understanding of the process.

Conclusions

Despite the extensive literature on the direct synthesis this is the first time that three different reactors are compared using the same catalyst and similar reaction conditions. The corresponding Arrhenius parameters were estimated from direct synthesis experiments for all the reactions and reactors. Comparable activation energies were seen for H_2O_2 synthesis in batch and semibatch reactors, 42.6 and 67.0 kJ/mol respectively while the one in the TBR was 6.9 kJ/mol, and thus the direct synthesis rate in the TBR was almost independent from the temperature. Direct water formation activation energies were quite high in batch and semibatch showing that this reaction rate is becomes very important with the increase of the temperature. In the TBR the activation energy for water formation is close to the activation energy of the direct synthesis. It was already clear that the hydrogenation and decomposition can be avoided with the temperature, here we found that in batch and semibatch the temperature plays a big role while in the case of a TBR operated in mass transfer the temperature is not affecting so much the decomposition and hydrogenation. These information remark the importance of the direct water formation in the TBR, while in the batch and semibatch this effect is less pronounced, especially in semibatch. Hydrogenation and decomposition have little effect in the batch and semibatch and also in the TBR. It is very interesting to see how the direct water formation rate is more pronounced when the reaction is operated mass transfer

regime. Important guidelines are gained to operate continuously and to enhance the H_2O_2 production in the TBR reactor. To avoid the H_2O formation in a continuous reactor short contact time is needed coupled probably with a gas-liquid recirculation, this will help to enhance the H_2O_2 production avoiding the water formation. The environment should be kept always with a high concentration of hydrogen in the liquid phase and thus favoring the H_2O_2 production. Multiple injection points in the continuous reactor will favor the control of the H_2 dosing and keeping high concentration of hydrogen in the liquid phase avoiding working in the flammability limits. Once through reactor for commercialization purpose is impossible at the present moment. The catalyst development should not only take into account the Pd (or PdAu) state of oxidation and nanocluster size but also the porosity of the support and the effect of the mass transfer in the supporting material. Indeed, as we have seen in the TBR, the mass transfer plays an important role, and tailoring the porosity of the support could be a fundamental aspect to improve the catalyst for a continuous reactor.

The direct synthesis possibly passes through the limitation of the PdO sites that seem responsible of the water formation (direct combustion). The hydrogenation seems more dependent on the H_2O_2 concentration and the dynamics of H_2/O_2 adsorption on the catalyst surface.

Moreover it is important to take into consideration the reactor used to fully understand the environment conditions that can affect the reaction rate (i.e. the dynamics on the nanoclusters surface).

These new findings will help to design new catalysts and to perform the reaction with a chemical reaction engineering point of view, maximizing the reactor design and performances. To conclude, the catalyst design should be made according to the features of the reactor and not only looking at the catalyst itself.

Nomenclature

Dimensionless number

Ga Galilei number, TBR model ($d_p^3 g \rho_L^2/\mu_L^2$)

Pe Peclet number, TBR model ($\mu_L d_p/\mathcal{D}$)

Re_{Gp} Reynolds number of the gas and particle, TBR model ($\rho_G u_G d_p/\mu_G$)

Re_{Lp} Reynolds number of the liquid and particle, TBR model ($\rho_L u_L d_p/\mu_L$)

Greek letters

ε bed porosity in the trickle bed reactor (0.33, dimensionless)

μ_G gas viscosity (g/(cm·s))

μ_L liquid viscosity (g/(cm·s))

ρ_B catalyst density in the liquid phase (g/cm^3)

ρ_G gas density (g/cm^3)

ρ_L liquid density (g/cm^3)

τ residence time, eq. (26) (s)

ϑ dimensionless residence time, TBR model

Symbols

A_i Pre-exponential factor of reaction i

C concentration (mol/cm^3)

d_p equivalent diameter of particle, TBR model (cm)

$\mathcal{D}$ axial dispersion, TBR model (cm^2/s)

err, err_T error function total and at a given temperature, respectively (dimensionless)

Ea_i Activation energy of reaction i

g gravitational acceleration (9.066 m/s)

H Henry constant, eq. (16) (dimensionless)

$k_i a^{LG}$ gas-liquid mass transfer coefficient (s^{-1})

k kinetic constant

L length of the trickle bed reactor (cm)

n moles (mol)

$\dot{n}$ molar flow, semibatch model (mol/s)

N number of experimental data, eq. (33)

r specific production rate ($mol/(s\, g_{CAT})$)

R specific reaction rate ($mol/(s\, g_{CAT})$)

S selectivity (%)

t time coordinate (s)

u_G superficial gas velocity, TBR model (cm/s)

u_L superficial liquid velocity, TBR model (cm/s)

V volume (cm^3)

$\dot{V}$ volumetric flow, TBR model (cm^3/s)

X_{H_2} H_2 conversion (%)

z dimensionless space coordinate, TBR model

Subscripts

$i,\ i$th species

Tot total

ds, wf, d, h direct synthesis, water formation, disproportionation and hydrogenation reactions, respectively

Superscripts

ADM axial dispersion model, TBR model

calc calculated

exp experimental

G gas

IN inlet

L liquid

OUT outlet

ST stirred tank model, TBR model

* gas-liquid equilibrium

Acknowledgements

References

1 G. Centi, S. Perathoner and S. Abate, in *Modern Heterogeneous Oxidation Catalysis*, ed. nonymous , Wiley-VCH Verlag GmbH & Co. KGaA, 2009, p. 253-287.

2 C. Samanta, *Applied Catalysis A: General,* 2008, **350**, 133-149 (DOI:10.1016/j.apcata.2008.07.043).

3 J. Garcia-Serna, T. Moreno, P. Biasi, M. J. Cocero, J. Mikkola and T. O. Salmi, *Green Chem.,* 2014, **16**, 2320 (DOI:10.1039/C3GC41600C).

4 J. K. Edwards, S. J. Freakley, R. J. Lewis, J. C. Pritchard and G. J. Hutchings, *Catalysis Today,* 2015, **248**, 3-9 (DOI:http://dx.doi.org/10.1016/j.cattod.2014.03.011).

5 T. Inoue, J. Adachi, K. Ohtaki, M. Lu, S. Murakami, X. Sun and D. F. Wang, *Chem. Eng. J.,* 2015, **278**, 517-526 (DOI:http://dx.doi.org/10.1016/j.cej.2014.11.019).

6 T. Salmi, N. Gemo, P. Biasi and J. G. Serna, *Catalysis Today,* 2015, **248**, 108-114 (DOI:http://dx.doi.org/10.1016/j.cattod.2014.03.020).

7 F. Menegazzo, M. Manzoli, M. Signoretto, F. Pinna and G. Strukul, *Catalysis Today,* 2015, **248**, 18-27 (DOI:http://dx.doi.org/10.1016/j.cattod.2014.01.015).

8 J. K. Edwards, S. F. Parker, J. Pritchard, M. Piccinini, S. J. Freakley, Q. He, A. F. Carley, C. J. Kiely and G. J. Hutchings, *Catal. Sci. Technol.,* 2013, **3**, 812-818 (DOI:10.1039/C2CY20767B).

9 P. Biasi, S. Sterchele, F. Bizzotto, M. Manzoli, S. Lindholm, P. Ek, J. Bobacka, J. Mikkola and T. Salmi, *Catalysis Today,* 2015, **246**, 207-215 (DOI:http://dx.doi.org/10.1016/j.cattod.2014.11.027).

10 M. Sankar, Q. He, M. Morad, J. Pritchard, S. J. Freakley, J. K. Edwards, S. H. Taylor, D. J. Morgan, A. F. Carley, D. W. Knight, C. J. Kiely and G. J. Hutchings, *ACS Nano,* 2012, **6**, 6600-6613 (DOI:10.1021/nn302299e).

11 R. Arrigo, M. E. Schuster, S. Abate, S. Wrabetz, K. Amakawa, D. Teschner, M. Freni, G. Centi, S. Perathoner, M. Hävecker and R. Schlögl, *ChemSusChem,* 2014, **7**, 179-194 (DOI:10.1002/cssc.201300616).

12 S. Abate, M. Freni, R. Arrigo, M. E. Schuster, S. Perathoner and G. Centi, *ChemCatChem,* 2013, **5**, 1899-1905 (DOI:10.1002/cctc.201200914).

13 J. K. Edwards, A. Thomas, A. F. Carley, A. A. Herzing, C. J. Kiely and G. J. Hutchings, *Green Chem.,* 2008, **10**, 388-394.

14 G. Blanco-Brieva, F. E. de, J. Campos-Martin and J. L. G. Fierro, *Green Chem.,* 2010, **12**, 1163-1166 (DOI:10.1039/C003700A).

15 S. Kim, D. Lee and K. Lee, *Journal of Molecular Catalysis A: Chemical,* 2014, **383–384**, 64-69 (DOI:http://dx.doi.org/10.1016/j.molcata.2013.11.021).

16 Q. Liu, K. Gath, J. Bauer, R. Schaak and J. Lunsford, *The Active Phase in the Direct Synthesis of H_2O_2 from H_2 and O_2 over Pd/SiO_2 Catalyst in a H_2SO_4/Ethanol System*, Springer Netherlands, 2009.

17 G. Blanco-Brieva, E. Cano-Serrano, J. Campos-Martin and J. L. G. Fierro, *Chem. Commun.,* 2004, **0**, 1184-1185.

18 J. K. Edwards, J. Pritchard, P. J. Miedziak, M. Piccinini, A. F. Carley, Q. He, C. J. Kiely and G. J. Hutchings, *Catal. Sci. Technol.,* 2014, **4**, 3244-3250 (DOI:10.1039/C4CY00496E).

19 F. Menegazzo, M. Signoretto, M. Manzoli, F. Boccuzzi, G. Cruciani, F. Pinna and G. Strukul, *Journal of Catalysis,* 2009, **268**, 122-130.

20 F. Menegazzo, P. Burti, M. Signoretto, M. Manzoli, S. Vankova, F. Boccuzzi, F. Pinna and G. Strukul, *Journal of Catalysis,* 2008, **257**, 369-381.

21 E. N. Ntainjua, M. Piccinini, J. C. Pritchard, J. K. Edwards, A. F. Carley, C. J. Kiely and G. J. Hutchings, *Catalysis Today,* 2011, **178**, 47-50.

22 J. C. Pritchard, Q. He, E. N. Ntainjua, M. Piccinini, J. K. Edwards, A. A. Herzing, A. F. Carley, J. A. Moulijn, C. J. Kiely and G. J. Hutchings, *Green Chem.,* 2010, **12**, 915-921.

23 S. Abate, R. Arrigo, S. Perathoner and G. Centi, *Topics in Catalysis,* 2014, , 1-10 (DOI:10.1007/s11244-014-0289-1).

24 M. Piccinini, J. K. Edwards, J. A. Moulijn and G. J. Hutchings, *Catal. Sci. Technol.,* 2012, **2**, 1908-1913.

25 R. Dittmeyer, J. -. Grunwaldt and A. Pashkova, *Catalysis Today,* 2014, , (DOI:http://dx.doi.org/10.1016/j.cattod.2014.03.055).

26 P. Biasi, J. Garcia-Serna, A. Bittante and T. Salmi, *Green Chem.,* 2013, **15**, 2502-2513 (DOI:10.1039/C3GC40811F).

27 S. J. Freakley, M. Piccinini, J. K. Edwards, E. N. Ntainjua, J. A. Moulijn and G. J. Hutchings, *ACS Catal.,* 2013, **3**, 487-501 (DOI:10.1021/cs400004y).

28 P. Biasi, F. Menegazzo, F. Pinna, K. Eränen, P. Canu and T. O. Salmi, *Ind. Eng. Chem. Res.,* 2010, **49**, 10627-10632.

29 V. Paunovic, J. C. Schouten and T. A. Nijhuis, *Catalysis Today;,* 2015, **248**, 160-168 (DOI:http://dx.doi.org/10.1016/j.cattod.2014.04.007).

30 T. Deguchi, H. Yamano and M. Iwamoto, *Catalysis Today,* 2015, **248**, 80-90 (DOI:http://dx.doi.org/10.1016/j.cattod.2014.04.008).

31 N. Gemo, P. Biasi, P. Canu and T. O. Salmi, *Chemical Engineering Journal,* 2012, **207–208**, 539-551 (DOI:10.1016/j.cej.2012.07.015).

32 Y. Voloshin and A. Lawal, *Chemical Engineering Science,* 2010, **65**, 1028-1036 (DOI:10.1016/j.ces.2009.09.056).

33 P. Biasi and J. G. Serna, *Catalysis Today,* 2015, **248**, 1-2 (DOI:http://dx.doi.org/10.1016/j.cattod.2015.03.008).

34 N. Gemo, S. Sterchele, P. Biasi, P. Centomo, P. Canu, M. Zecca, A. Shchukarev, K. Kordas, T. O. Salmi and J. Mikkola, *Catal. Sci. Technol.,* 2015, **5**, 3545-3555 (DOI:10.1039/C5CY00493D).

35 P. Biasi, F. Menegazzo, F. Pinna, K. Eränen, T. O. Salmi and P. Canu, *Chem. Eng. J.,* 2011, **176-177**, 172-177.

36 S. Sterchele, P. Biasi, P. Centomo, P. Canton, S. Campestrini, T. Salmi and M. Zecca, *Applied Catalysis A: General,* 2013, **468**, 160-174 (DOI:http://dx.doi.org/10.1016/j.apcata.2013.07.057).

37 C. Burato, S. Campestrini, Y. Han, P. Canton, P. Centomo, P. Canu and B. Corain, *Applied Catalysis A: General,* 2009, **358**, 224-231 (DOI:10.1016/j.apcata.2009.02.016).

38 C. Burato, P. Centomo, M. Rizzoli, A. Biffis, S. Campestrini and B. Corain, *Advanced Synthesis & Catalysis,* 2006, **348**, 255-259 (DOI:10.1002/adsc.200505208).

39 N. Gemo, P. Biasi, T. O. Salmi and P. Canu, *The Journal of Chemical Thermodynamics,* 2012, **54**, 1-9 (DOI:10.1016/j.jct.2012.03.021).

40 P. Biasi, N. Gemo, J. R. Hernández Carucci, K. Eränen, P. Canu and T. O. Salmi, *Industrial and Engineering Chemistry Research,* 2012, **51**, 8903-8912 (DOI:10.1021/ie2021398).

41 A. Bernardini, N. Gemo, P. Biasi, P. Canu, J. P. Mikkola, T. Salmi and R. Lanza, *Catalysis Today,* (DOI:http://dx.doi.org/10.1016/j.cattod.2014.12.033).

42 T. Deguchi and M. Iwamoto, *Journal of Catalysis,* 2011, **280**, 239-246 (DOI:10.1016/j.jcat.2011.03.019).

43 D. P. Dissanayake and J. H. Lunsford, *Journal of Catalysis,* 2003, **214**, 113-120 (DOI:10.1016/S0021-9517(02)00171-9).

44 C. Sivadinarayana, T. V. Choudhary, L. L. Daemen, J. Eckert and D. W. Goodman, *J. Am. Chem. Soc.,* 2004, **126**, 38-39 (DOI:10.1021/ja0381398).

45 N. M. Wilson and D. W. Flaherty, *J. Am. Chem. Soc.,* 2015, (DOI:10.1021/jacs.5b10669).

46 A. Bittante, J. García-Serna, P. Biasi, F. Sobrón and T. Salmi, *Chem. Eng. J.,* 2014, **250**, 99-111 (DOI:http://dx.doi.org/10.1016/j.cej.2014.03.062).

47 J. K. Edwards, J. Pritchard, M. Piccinini, G. Shaw, Q. He, A. F. Carley, C. J. Kiely and G. J. Hutchings, *Journal of Catalysis,* 2012, **292**, 227-238 (DOI:10.1016/j.jcat.2012.05.018).

48 V. Choudhary, A. Gaikwad and S. Sansare, *Catalysis Letters,* 2002, **83**, 235-239 (DOI:10.1023/A:1021066904862).

49 V. R. Choudhary, S. D. Sansare and A. G. Gaikwad, *Catalysis Letters,* 2002, **84**, 81-87.

50 S. Melada, R. Rioda, F. Menegazzo, F. Pinna and G. Strukul, *Journal of Catalysis,* 2006, **239**, 422-430 (DOI:10.1016/j.jcat.2006.02.014).

51 J. Hinojosa Jose A., H. H. Kan and J. F. Weaver, *J. Phys. Chem. C,* 2008, **112**, 8324-8331 (DOI:10.1021/jp800216x).

52 D. Zemlyanov, B. Klötzer, H. Gabasch, A. Smeltz, F. Ribeiro, S. Zafeiratos, D. Teschner, P. Schnörch, E. Vass, M. Hävecker, A. Knop-Gericke and R. Schlögl, *Topics in Catalysis,* 2013, **56**, 885-895 (DOI:10.1007/s11244-013-0052-z).

53 G. W. Simmons, Y. N. Wang, J. Marcos and K. Klier, *J. Phys. Chem.,* 1991, **95**, 4522-4528 (DOI:10.1021/j100164a063).

54 A. N. Salanov, A. I. Titkov and V. N. Bibin, *Kinetics and Catalysis,* 2006, **47**, 430-436 (DOI:10.1134/S0023158406030153).

55 E. Rangel, L. F. Magana and L. E. Sansores, *ChemPhysChem,* 2014, **15**, 4042-4048 (DOI:10.1002/cphc.201402532).

56 I. Meusel, J. Hoffmann, J. Hartmann, M. Heemeier, M. Bäumer, J. Libuda and H. -. Freund, *Catalysis Letters,* 2001, **71**, 5-13 (DOI:10.1023/A:1016635804185).

57 M. Shao, T. Yu, J. H. Odell, M. Jin and Y. Xia, *Chem. Commun.,* 2011, **47**, 6566-6568 (DOI:10.1039/C1CC11004G).

58 J. Zou, S. G. Stewart, C. L. Raston and K. S. Iyer, *Chem. Commun.,* 2011, **47**, 1803-1805 (DOI:10.1039/C0CC03182H).

59 L. Ouyanga, , P.-f. Tiana, G.-j. Daa, X.-C. Xua, C. Aoa, T.-y. Chena, R. Sib, J. Xua, Y.-F. Han, J.Cat., 2015, 321, 70-80. (DOI: doi:10.1016/j.jcat.2014.10.003)

The analysis of hydrogen peroxide direct synthesis in three different reactors reveals new insight on the mechanism of this challenging reaction.

$$H_2$$

$$+1/2\,O_2 \rightarrow H_2O$$

$$+O_2 \rightarrow H_2O_2$$

$$+ H_2 \rightarrow 2H_2O$$

$$\rightarrow H_2O + 1/2\,O_2$$